www.czasopisma.pan.pl PAN POLSKA AKADEMIA NAUK www.journals.pan.pl

ARCHIVES OF ACOUSTICS Vol. 48, No. 1, pp. 49–61 (2023), doi: 10.24425/aoa.2022.142909

Research Paper

Using SVM Classifier and Micro-Doppler Signature for Automatic Recognition of Sonar Targets

Abbas SAFFARI[(1)], Seyed Hamid ZAHIRI[(1)*], Navid KHOZEIN GHANAD[(2)]

[(1)] *University of Birjand*
Birjand, Iran

[(2)] *Sajjad University of Mashhad*
Mashhad, Iran

*Corresponding Author e-mail: hzahiri@birjand.ac.ir

(*received September 20, 2021; accepted August 29, 2022*)

In this paper, we propose using a propeller modulation on the transmitted signal (called sonar micro-Doppler) and different support vector machine (SVM) kernels for automatic recognition of moving sonar targets. In general, the main challenge for researchers and craftsmen working in the field of sonar target recognition is the lack of access to a valid and comprehensive database. Therefore, using a comprehensive mathematical model to simulate the signal received from the target can respond to this challenge. The mathematical model used in this paper simulates the return signal of moving sonar targets well. The resulting signals have unique properties and are known as frequency signatures. However, to reduce the complexity of the model, the 128-point fast Fourier transform (FFT) is used. The selected SVM classification is the most popular machine learning algorithm with three main kernel functions: RBF kernel, linear kernel, and polynomial kernel tested. The accuracy of correctly recognizing targets for different signal-to-noise ratios (SNR) and different viewing angles was assessed. Accuracy detection of targets for different SNRs (−20, −15, −10, −5, 0, 5, 10, 15, 20) and different viewing angles (10, 20, 30, 40, 50, 60, 70, 80) is evaluated. For a more fair comparison, multilayer perceptron neural network with two back-propagation (MLP-BP) training methods and gray wolf optimization (MLP-GWO) algorithm were used. But unfortunately, considering the number of classes, its performance was not satisfactory. The results showed that the RBF kernel is more capable for high SNRs (SNR = 20, viewing angle = 10) with an accuracy of 98.528%.

Keywords: sonar micro-Doppler; automatic recognition; SVM; RBF kernel; linear kernel; polynomial kernel.

1. Introduction

Due to the increasing use of automatic target recognition systems in various military and commercial industries, the issue of classification and automatic target recognition has become one of the favorite interests of craftsmen and activists in this field (EHRMAN, LANTERMAN, 2020; SMITH *et al.*, 2007). The most important advantage of using these systems is eliminating the human role from the target identification and detection processes (BHANU, 1986). One of the most important reasons for replacing these systems with systems controlled by human operators is a slow human reaction, low reliability, and high dependence on mental conditions (ZHOU *et al.*, 2022). The main element of many defense and military missions in the sea is the automatic detection and identification of sonar targets (LIU *et al.*, 2019). The complex physical properties of sonar targets and the heterogeneous conditions of sound propagation at sea have led to many features being extracted to identify and detect sonar targets (KHISHE, SAFARI, 2019). Obviously, with increasing the dimensions of the feature vector, the dimensions of the data also increase (SAFFARI *et al.*, 2022a).

The first challenge that sonar researchers face is obtaining reliable datasets (DONG *et al.*, 2021; GLOVER, LAGUNA, 2008). Creating a sonar dataset generates high costs (CHEN *et al.*, 2022; WAITE, 2002). According to the research, the sonar datasets are usually acquired by performing a sonar collection scenario

in a real environment (Kaveh *et al.*, 2019; Qiao *et al.*, 2021; Saffari *et al.*, 2022b; Wu *et al.*, 2021). Another solution for collecting sonar datasets is to use a cavitation tunnel (Khishe, Mosavi, 2019; Khishe, Mohammadi, 2019; Khishe, Safari, 2019). The most important disadvantage of using these methods is the presence of noise in the environment. In other words, the dataset is reliable and can be used for practical systems that perform well even in high-noise environments. One of the main motivations of this paper is to provide a practical model for simulating the emitted signals from sonar targets with the ability to adjust the SNR value and the target angle of view of the sonar receiver.

The next step after preparing the data is extracting the signal's attribute. All submarines have propellers for propulsion. When acoustic signals are propagated toward the target (floating propeller), the propeller's rotation reflects the transmitted signal (Clemente *et al.*, 2013). It can be said that this signal is unique; in other words, it is known as the corresponding floating frequency signature (Chen, Li, 2022; Tahmoush, 2015). The phenomenon of modulation of rotating parts (propeller) is known as sonar micro-Doppler. This phenomenon, called radar micro-Doppler, is widely used to classify aerial targets such as helicopters (Anderson, 2004; Mamgain *et al.*, 2018) and ground targets such as tanks (Foued *et al.*, 2017; Molchanov *et al.*, 2013). Unfortunately, we have not found any researches on the classification of sonar targets and in particular naval vessels using sonar micro-Doppler. Therefore, one of the main goals of this research is to investigate the effect of using this method in the automatic recognition of sonar targets for practical application.

The next step after feature extraction is the classifier design. There are two general approaches to classifying data (Koturwar *et al.*, 2015). The first method is to use definitive computational methods, which have very high reliability and definitely achieve the best results, but the disadvantage of these methods is clearly seen when the size of the data increases (such as sonar dataset). Then the spatial and temporal complexity increases (Lakhwani, 2020). Therefore, this method does not work well for sonar data (Cai *et al.*, 2021). The second approach is to use artificial intelligence (Jin *et al.*, 2020). The main subset of artificial intelligence is machine learning (Liu *et al.*, 2019; Sclavounos, Ma, 2018). One of the most popular supervised learning algorithms is support vector machine (SVM) (Uddin *et al.*, 2019). SVM has a relatively simple training phase and, unlike neural networks, does not fall into local maxima (Xu *et al.*, 2019). In addition, it works relatively well for high-dimensional data and, despite providing the optimal answer, has less time and space complexity than specific methods (Berthold *et al.*, 2018; Gaye *et al.*, 2021). According to the explanations given in this paper, sonar micro-Doppler and SVM will be used for the automatic recognition of sonar targets. In order to have a fair and comprehensive comparison, considering that in references (Saffari *et al.*, 2022c; 2022d) artificial neural network has been used to classify sonar targets, in this article (Kazimierski, Zaniewicz, 2021), two types of MLP-NNs with two types of BP and GWO training are used (Wawrzyniak, Stateczny, 2017; Zhang *et al.*, 2020).

The paper is organized in such a way that the second part explains SVM. In the third section, the micro-Doppler phenomenon is introduced. The fourth part introduces the automatic sonar detection system using sonar micro-Doppler. In the fifth part, the simulation results are presented. The sixth part is the conclusion.

2. Support vector machines

SVMs are supervised learning algorithms and a subset of heuristic algorithms (Kavzoglu, Colkesen, 2009). In SVM, hyperplanes usually separate the two classes and the training data set of a hyperplane are determined. The generalizability can then be verified using the test dataset. SVMs have been able to perform powerfully in many applications (Uddin *et al.*, 2019; Xu *et al.*, 2019).

To classify a data set with dimensional D, a *D-1* hyperplane is required. Figure 1 shows the different hyperplanes separating two different classes. However, only one optimal hyperplane divides data into two classes with the longest distance (Fig. 2). All points that limit the width of the margin are called support vectors. SVMs in binary class mode seek to find a hyperplane so that the distance between the members of each class to the optimal hyperplane is maximum. For example, it is assumed that a set of training data with a D sample is represented by $\{x_i, y_i\}$ and $(I = 1, 2, ..., D)$, where $x \in R^D$ is a D-dimensional space and $y \in \{-1, +1\}$ is a class label (Kavzoglu, Colkesen, 2009). The optimal hyperplane performance is to maximize margins. This hyperplane is defined as $w \cdot x_i + b = 0$, where w determines the orientation of the hyperplane in space, x is the points on the hyperplane, b is the bias of the distance of hyperplane

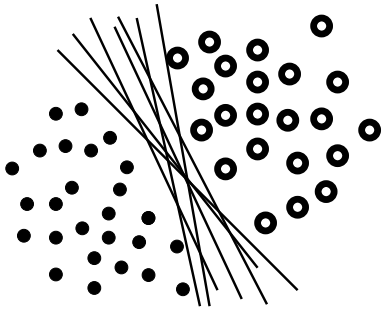

Fig. 1. Linear separation of data by different hyperplanes.

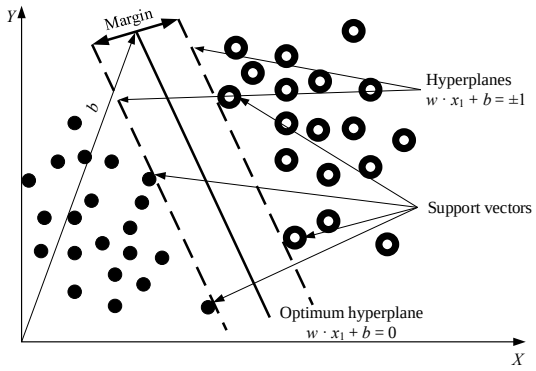

Fig. 2. Optimum hyperplane and support vectors for linearly separable data.

from the origin (Fig. 2). Equations (1) and (2) are the equations of a separating hyperplane for the separable state of two classes:

$$w \cdot x_i + b \geq +1 \qquad \text{for all} \quad y = +1, \tag{1}$$

$$w \cdot x_i + b \leq -1 \qquad \text{for all} \quad y = -1. \tag{2}$$

The aforementioned inequalities can be summed up in relation (3):

$$y_i(w \cdot x_i + b) - 1 \geq 0. \tag{3}$$

Support vectors are all points that exist in two parallel hyperplanes with the optimal hyperplane and are defined by the function $(w \cdot x_i + b) \pm 1 = 0$. If there is a hyperplane and Eq. (3) is established, the classes are separated linearly. Therefore, the margin between these aircrafts is $2/\|w\|$, distance to the nearest point. Minimize $\|w\|^2$ with the limit of Eq. (3) found the optimal hyperplane. Therefore, the following optimization problem must be solved to calculate the optimal aircraft hyperplane:

$$\min\left[\frac{1}{2}\|w\|^2\right]. \tag{4}$$

Of course subject to restrictions:

$$w \cdot x_i + b \geq 1 \qquad \text{and} \qquad y \in \{-1, +1\}. \tag{5}$$

Figure 3 shows the classification of separable nonlinear data. For such data, it is certainly not possible to

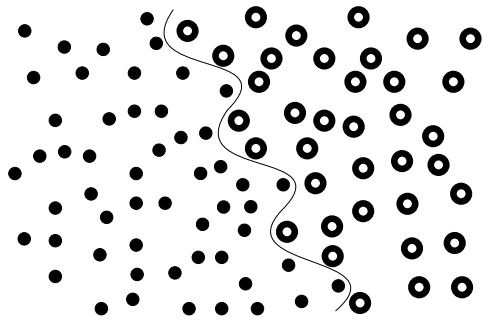

Fig. 3. Nonlinear separation of data.

classify data in two classes linearly. Therefore, in such cases where it is not possible to use a hyperplane with linear equations on the data, nonlinear decision levels should be used. Therefore, ξ slack variables replace the optimization problem (Fig. 4):

$$\min\left[\frac{\|w\|^2}{2} + C\sum_{i=1}^{r}\xi_i\right],$$

considering the following limitations:

$$y_i(w \cdot x_i + b) \geq 1 - \xi_i, \quad \xi_i \geq 0, \quad i = 1, 2, ..., N, \tag{6}$$

where C is a constant parameter and balances between two criteria, error minimization and margin maximization. Slack variables ξ_i show the distance of classified points from the optimal hyperplane cloud. If it is not possible to use a hyperplane with linear equations, it may be mapped into a high-dimensional space ($\circ D$) through some nonlinear mapping functions ($\varnothing$).

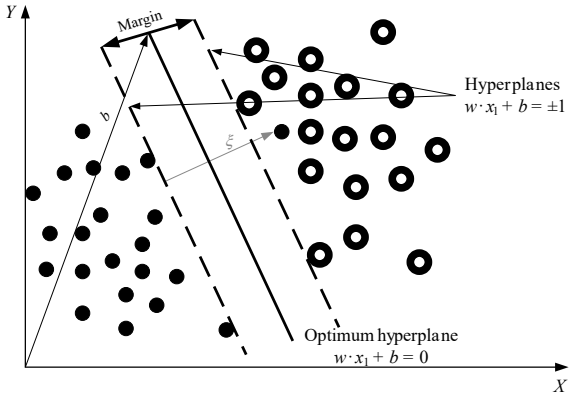

Fig. 4. Introducing slack variable for nonlinear data and generalization of the solution.

As shown in Fig. 5, the point x can be represented as $\varnothing(x)$ in the feature space. Complex computations $(\varnothing(x) \cdot \varnothing(x_i))$ are reduced using a kernel function. Therefore, the decision function for classification is as follows:

$$f(x) = \text{sign}\left(\sum_{i}^{z} a_i y_i \cdot K(X, X_i) + b\right), \tag{7}$$

where each z of the training case, there are X_i vectors that indicate the spectral response, $a_i y_i$ are Lagrange multipliers, and $K(X, X_i)$ is the kernel function, a_i depends on parameter C and its value is determined by it.

Kernel functions can be classified into four groups. In the following, 4 groups of SVM kernels are presented:

– linear kernel: the simplest kernel function is a linear kernel. Inner product of $X_i \cdot X_j$ and the constant coefficient C represent the linear kernel. Equation (8) represents the linear kernel function:

$$K(X_i, X_j) = X_i \cdot X_j; \tag{8}$$

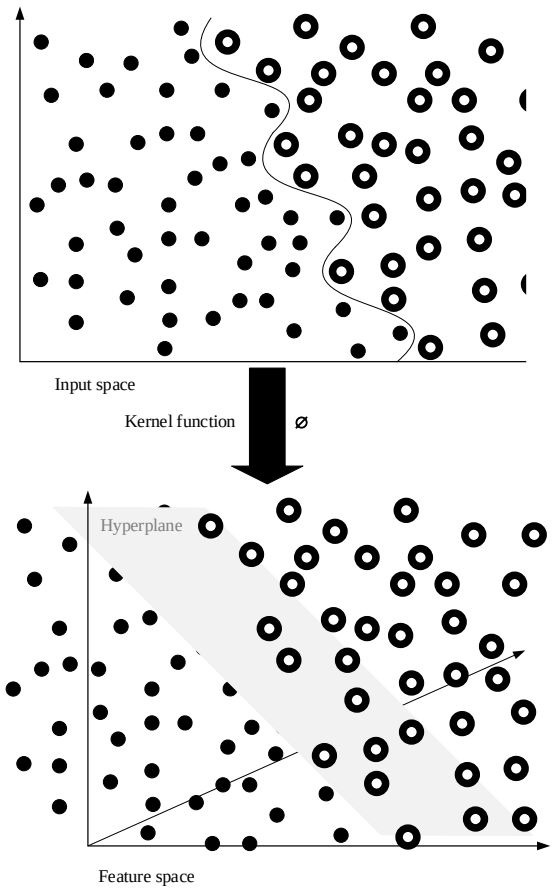

Fig. 5. Mapping of the data sets to the high-dimensional space with a kernel function.

– polynomial kernel: data separation is not possible linearly when useful features are not extracted or the amount of noise is high. To solve this problem, data must be mapped in different feature spaces so that they can be separated linearly. One of the kernel functions used in nonlinear separation is the polynomial kernel:

$$K\left(X_i, X_j\right) = \left(\gamma X_i \cdot X_j + C\right)^d, \tag{9}$$

where $C \geq 0$ represents a free parameter in the polynomial that trades off the impact of higher-order versus lower order terms;

– RBF kernel: the Gaussian kernel or RBF kernel is shown in Eq. (10):

$$K_{\mathrm{RBF}}\left(X_i, X_j\right) = \exp\left(-\gamma \left|X_i \cdot X_j\right|^2\right), \tag{10}$$

where γ is a parameter that used to set the spread of the kernel.

In this paper, the One-vs-All (OVA) method is used for classification.

3. Micro-Doppler

Micro-motions, such as vibrations or rotations of an object or structure on an object (Saffari *et al.*, 2022b; Yang *et al.*, 2006), cause changes in the extra frequencies on the signal, leading to sidebands on the object's Doppler frequency (Saffari *et al.*, 2022b; Tahmoush, 2015). This phenomenon is called sonar micro-Doppler. Recent research has shown that micro-Doppler techniques can identify or classify a target with its micro-Doppler properties. To explore the micro-Doppler properties of an object, time-frequency analysis is used to provide information about these local properties over time and frequency (Smith *et al.*, 2007). In most cases, the micro motion has a unique signature object. Micro-motion is created directly by the dynamic motion properties of an object, and the micro-Doppler properties are a direct reflection of micro-motion. Therefore, a micro-Doppler signature can be used to classify an object with unique motion characteristics (Yang *et al.*, 2006).

3.1. Theory

The analytic signal of a pure tone $s(t)$ is defined as the signal $\widehat{s}(t)$, such that $s(t)$ ¼ Real $\{\widehat{s}(t)\}$, and is generally expressed in a polar format as (Chen *et al.*, 2014):

$$\widehat{s}(t) = e^{j2\pi f_0 t}. \tag{11}$$

A target moving at a constant radial velocity u has the following Doppler shift relative to the sonar (or radar) system:

$$f_D = 2f_0 \frac{v}{C_s}, \tag{12}$$

where f_0 is the carrier frequency of the active sensor and C_s is the speed of propagation of sound in water (or air). If the target has a number M parts and each part moves at a velocity component $v_i(t)$, the Doppler shift is the sum of each single Doppler shift:

$$f_D(t) = \sum_{i=1}^{M} 2f_0 \frac{v_i(t)}{C_s}. \tag{13}$$

For such a target, the analytical signal of the echo return is as follows:

$$\widehat{s}_R\left(t\right) = e^{j2\pi f_0 t} \cdot e^{j2\pi f_D(t)t}. \tag{14}$$

Mixing the received signal $\hat{s}_R\left(t\right)$ with the conjugate of the transmitted signal $\hat{s}\left(t\right)$ is as follows:

$$\widehat{s}_R\left(t\right) \cdot \widehat{s}(t)^* = e^{j2\pi f_D(t)t}. \tag{15}$$

The aforementioned relation makes it possible to extract the Doppler signature from the data. This is the signal component that contains the micro-Doppler information on the target, which can be used for target recognition and classification.

4. Design of automatic sonar target recognition system using sonar micro-Doppler signature

Like any other pattern recognition system, designing an automatic sonar target recognition system has the following steps.

4.1. Data acquisition

One of the severe challenges for sonar research is the lack of reliable data. On the other hand, such things as the complex and heterogeneous environment of the sea, as well as the presence of unwanted signals in the sea (noise, clutter, and resonance) are the motivation for preparing a simulated data set using the mathematical model of the return signal of the rotation of the propeller. The targets tested are according to Table 1.

Table 1. Information on reference targets.

Number	Type	Model
1	Container ship	Emma Maersk
2	Container ship	MV Barzan
3	Container ship	MSC Oscar
4	Oil tanker	Front Century
5	Oil tanker	Seawise Giant
6	Passenger ship	Motorboat
7	Passenger ship	Oasis of the seas
8	Passenger ship	Leading Atlas
9	Cruise	Harmony of the Seas
10	Tugboat	ASD TUG 2913
11	Tugboat	Chinese oceanic tug boat
12	Research vessel	Nathaniel B. Palmer
13	Autonomous underwater vehicle	Tech 475 AUV
14	Military	Torpedo No. 1
15	Military	Torpedo No. 2
16	Military	Logistic Support
17	Military	Littoral Combat Ship No. 1
18	Military	Littoral Combat Ship No. 2
19	Military	Destroyer No. 1
20	Military	Destroyer No. 2
21	Military	Frigates
22	Military	Aircraft Carrier
23	Military	light submarine
24	Military	semi-heavy submarine
25	Military	heavy submarine

Different types of vessels were used in selecting the samples, including container vessels, tankers, passengers, cruises, autonomous underwater vehicles, tugboats, different classes of navy ships, submarines, and military torpedoes to evaluate the performance of the proposed model.

4.2. Extracting feature vectors

To generate a data set of return signals from the rotating part (propeller) of sonar targets, which is discussed in Subsec. 4.1, a suitable mathematical model (Eq. (16)) was used to simulate the return signal from the propeller:

$$s_r(t) = \sum_{n=0}^{N-1} A_r (L_2 - L_1) e^{j(\beta)} \cdot \operatorname{sinc}\left(\frac{4\pi}{\lambda}\frac{(L_2-L_1)}{2}\cos(\theta)\sin\left(\omega_r t + \frac{2\pi n}{N}\right)\right), \quad (16)$$

$$\beta = \omega_c t - \frac{4\pi}{\lambda} \cdot \left(R + vt + \frac{L_1+L_2}{2}\cos(\theta)\sin\left(\omega_r t + \frac{2\pi n}{N}\right)\right).$$

The parameters used in Eq. (16) are described in Table 2.

Table 2. Relationship parameters (16).

Parameters	Descriptions
$s_r(t)$	Return signal in time
N	Number of blades
A_r	A normalizing factor
L_1	The distance from the beginning of the blades to the center of rotation
L_2	The distance from the end of the blades to the center of rotation
ω_c	Radian frequency of the transmitted signal
λ	The wavelength of the transmitted signal
R	The distance from the center of rotation to the sonar receiver
v	Target speed relative to sonar receiver
θ	Target viewing angle
ω_r	Radian frequency of rotation

Figure 6 shows how to obtain a return signal using Eq. (16).

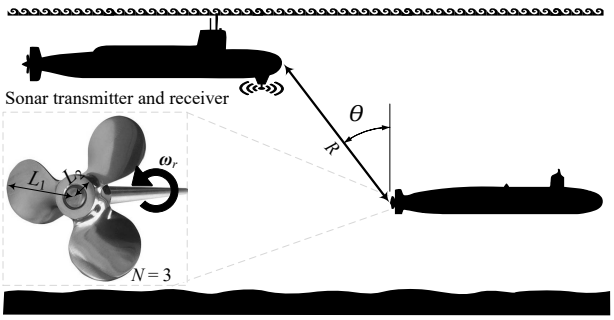

Fig. 6. How to obtain a return signal using Eq. (16).

The feature extracted from these signals is the Components 128-point from FFT. The structure of the feature vector expresses the target in the viewing angle (θ), and the SNR specified as follow:

$$\text{feature vector} = [f_1, f_2, f_3, ..., f_{126}, f_{127}, f_{128}]_{(\text{SNR},\theta)}, \quad (17)$$

where each of its components corresponds to a point of 128-point FFT in the angle of view and the specified SNR.

The reference classes correspond to the twenty-five objectives of Table 1. Samples of each class include feature vectors in nine SNRs (20, 15, 10, 5, 0, –5, –10, –15, and –20 dB) and eight viewing angles (10, 20, 30, 40, 50, 60, 70, and 80 degrees). Each class contains 30 samples in SNR and specified viewing angles. Thus, there are 2160 samples in each class (corresponding to each target) for all SNRs and viewing angles. In total, the dataset contains 54,000 samples.

Figure 7 shows samples of simulated acoustic signals and frequency signatures from sonar micro-Doppler at different SNRs for target No. 8.

Figure 8 shows the effect of the viewing angles on the return signal at SNR = –20 for target No. 8.

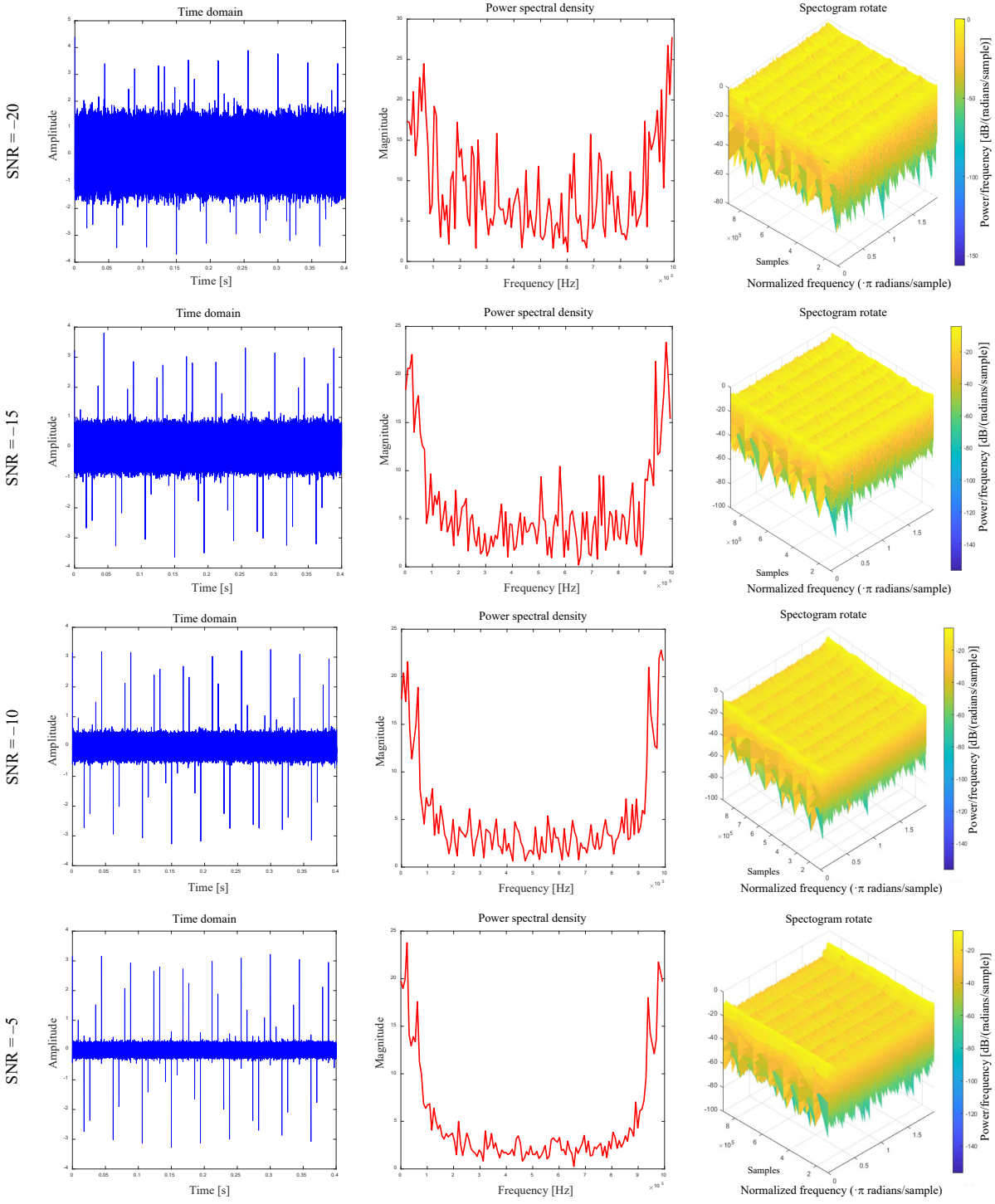

[Fig. 7.]

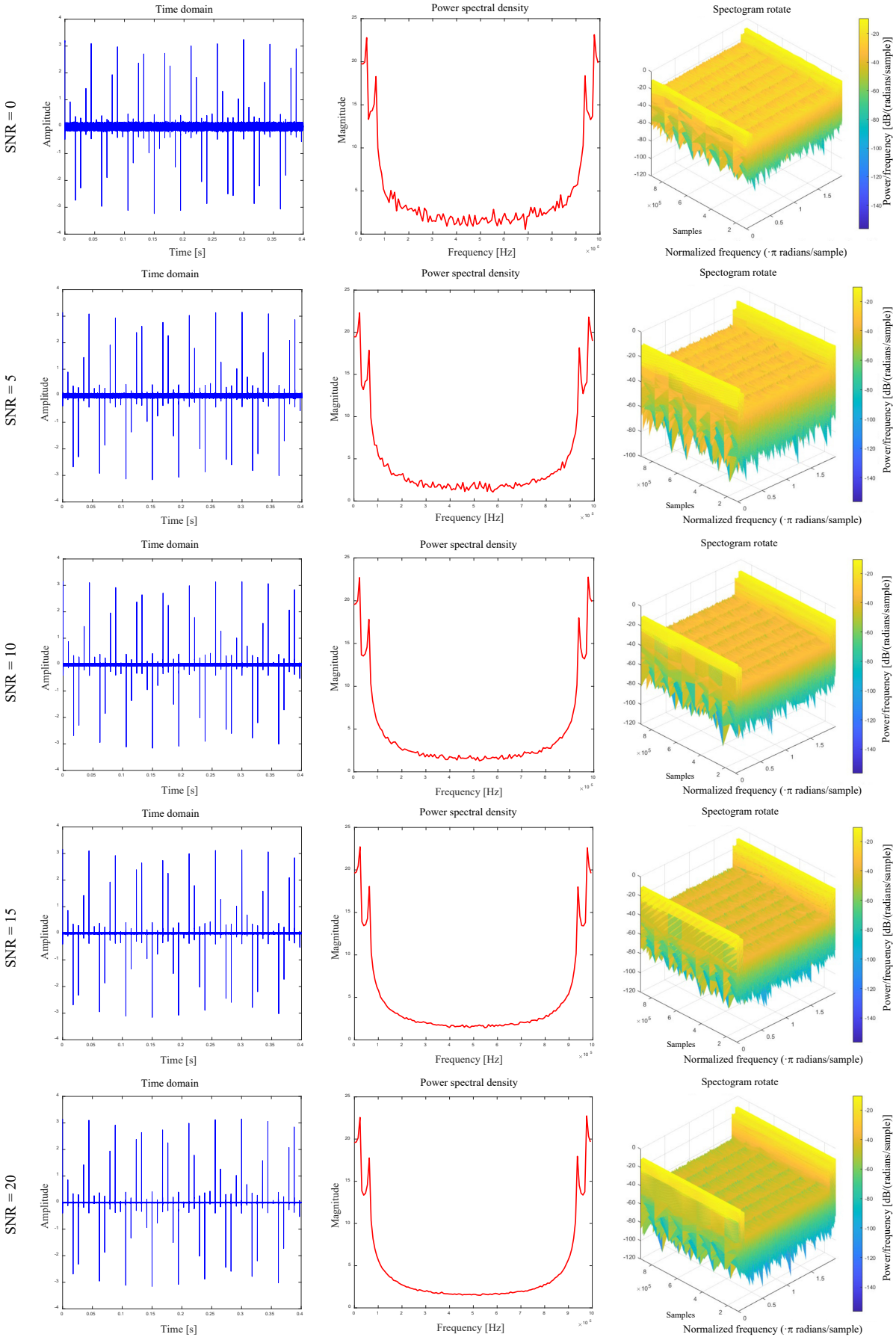

Fig. 7. Samples of simulated acoustic signals and frequency signatures of sonar micro-Doppler in different SNRs for target No. 8.

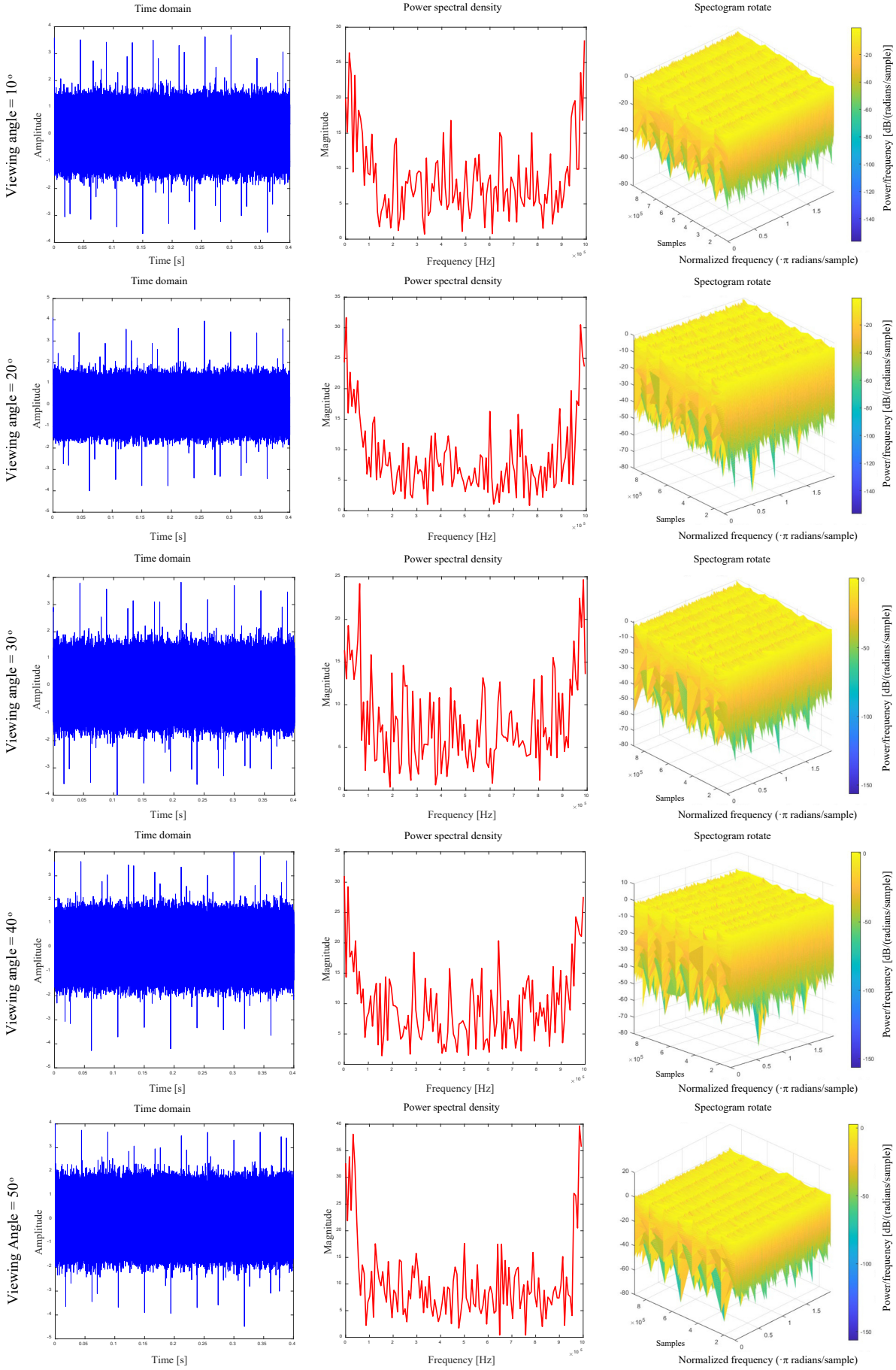
Viewing angle = 10°
Viewing angle = 20°
Viewing angle = 30°
Viewing angle = 40°
Viewing Angle = 50°
Time domain
Power spectral density
Spectogram rotate
Amplitude
Time [s]
Magnitude
Frequency [Hz]
Samples
Normalized frequency (·π radians/sample)
Power/frequency [dB/(radians/sample)]

[Fig. 8.]

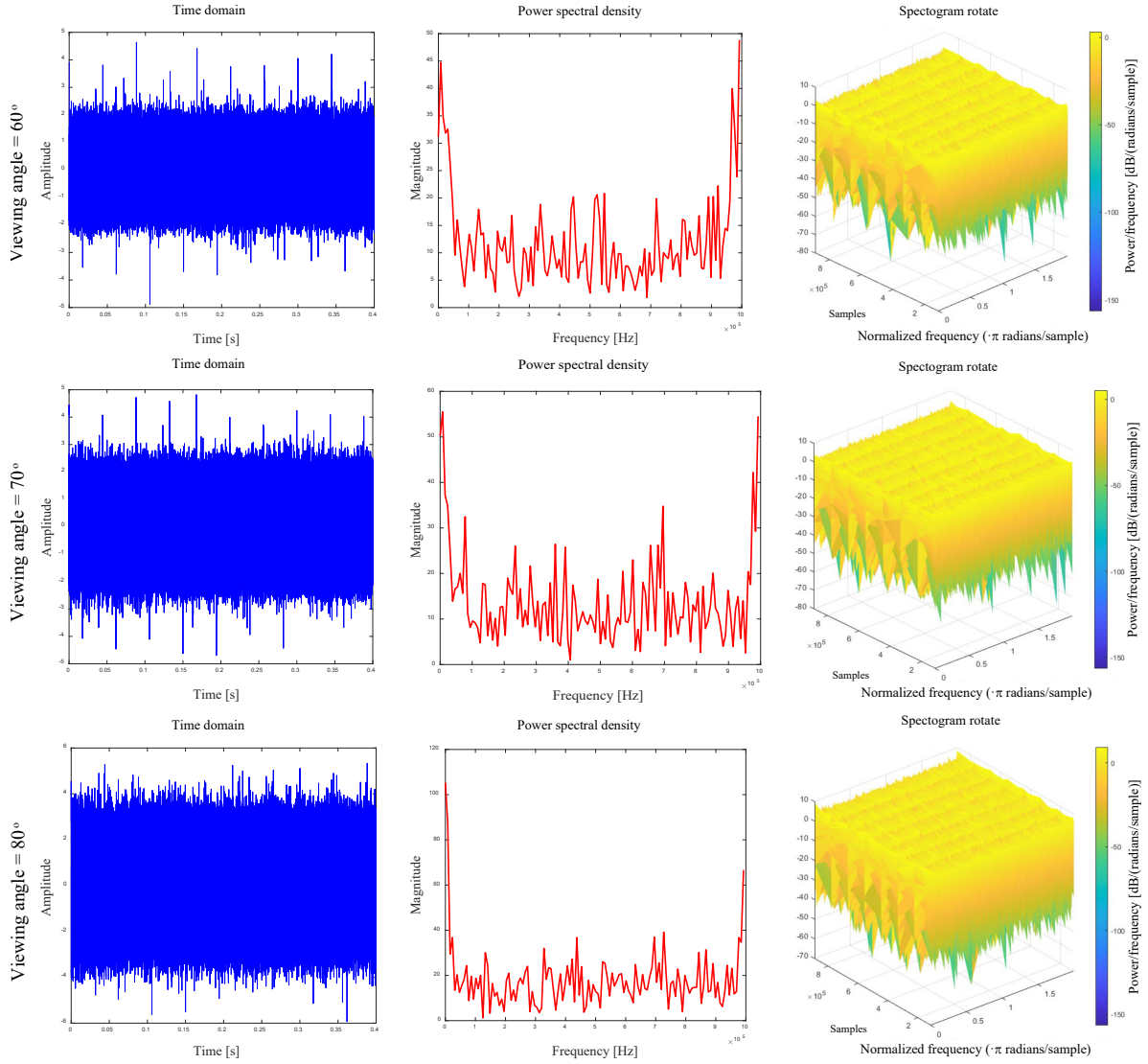

Fig. 8. Effect of the viewing angles on the return signal at SNR = −20 for target No. 8.

4.3. How to decide on a sonar target

This paper uses the three main kernel functions RBF, linear, and polynomial SVM classifier.

4.4. How to add noise

Noise mixed with the return signal from the target is assumed to be white Gaussian noise (Zhong *et al.*, 2022), and its random samples are simulated using uniform random variables. The power of the noise changes with the change of its variance. Different SNR ratios are performed by separately changing the noise power for each target. The signal strength for each target is its corresponding power at the same viewing angle.

5. Simulation results

In this section, the results obtained from the simulated system are analyzed. The results of the classification are the average of 15 program executions for each of the experiments. Each experiment assumes that the target angle of view and the SNR ratio is known. Due to the random nature of noise, in order to get the reference information in each SNR ratio as comprehensive as possible, the operation of generating random noise samples is performed 30 times. 70% of the samples are used to form a reference class related to a specific target and the other 30% are used as experimental data (unknown targets).

In general, according to the simulation results, it can be seen that in the SVM classifier, the RBF kernel works better for optimal conditions in which the noise level is lower. As the amount of noise increases, the linear kernel provides better results. Therefore, RBF, linear, and polynomial kernels performed better in terms of classification accuracy. Table 3 shows the results of the classification with the classifiers SVM-RBF, SVM-linear, and SVM-polynomial.

Table 3. The results of the classification with the classifiers SVM-RBF, SVM-linear, and SVM-polynomial.

SNR [dB]	Kernel	Angle 10°	Angle 20°	Angle 30°	Angle 40°	Angle 50°	Angle 60°	Angle 70°	Angle 80°
20	linear	93.008	92.016	91.696	90.160	90.192	88.672	86.960	81.520
	polynomial	94.432	94.800	94.096	92.736	92.480	91.440	84.592	77.872
	RBF	98.272	97.920	98.416	97.920	98.352	97.760	97.936	74.288
15	linear	92.688	92.032	91.088	90.272	91.136	87.776	84.864	79.056
	polynomial	92.016	92.096	91.840	90.672	90.848	88.864	80.480	70.656
	RBF	98.240	97.776	98.528	97.840	98.176	95.552	71.808	52.720
10	linear	92.144	91.600	89.088	89.088	88.640	86.720	81.968	75.024
	polynomial	87.824	87.600	86.384	85.536	84.048	82.416	74.432	64.144
	RBF	91.504	89.328	83.104	86.992	73.536	62.240	50.112	38.672
5	linear	90.032	89.760	87.136	88.832	86.992	82.688	75.664	75.488
	polynomial	81.904	82.176	79.136	81.264	78.448	71.328	63.200	58.096
	RBF	56.464	57.280	54.512	57.392	51.232	42.944	34.576	33.168
0	linear	82.912	83.936	83.984	80.464	81.056	77.072	74.208	64.256
	polynomial	70.240	71.216	71.248	69.488	70.912	64.640	59.488	53.136
	RBF	46.128	31.776	48.480	42.192	40.912	37.184	30.560	31.440
−5	linear	83.200	82.624	78.976	78.336	76.976	74.800	74.448	66.224
	polynomial	68.576	67.056	67.488	63.280	63.280	60.304	58.656	53.232
	RBF	38.720	34.720	39.312	38.720	35.424	43.904	38.960	44.992
−10	linear	70.864	69.520	67.584	65.680	69.488	70.944	66.816	68.560
	polynomial	53.776	52.384	50.080	51.040	50.816	50.784	51.136	48.656
	RBF	26.512	30.016	22.576	29.696	34.896	24.464	32.256	27.952
−15	linear	68.784	69.376	69.296	70.016	63.904	63.024	66.464	58.672
	polynomial	46.544	49.920	47.360	48.752	44.736	45.840	49.120	46.144
	RBF	25.808	24.544	28.496	30.992	22.208	24.832	15.104	12.688
−20	linear	70.112	73.568	69.312	67.840	67.440	66.752	64.576	62.304
	polynomial	48.160	45.056	48.656	46.800	45.072	48.128	52.208	49.568
	RBF	21.712	23.200	31.632	28.000	18.656	34.736	20.592	33.600

However, in terms of use in real environment with a lot of noise, linear, polynomial, and RBF kernels perform better.

Figure 9 shows the correct recognition rate for different SNR ratios at a 10° viewing angle for the three SVM classifier kernels, and Fig. 10 shows the correct recognition rate for different viewing angles at SNR = 20 dB for the three SVM classifier kernels.

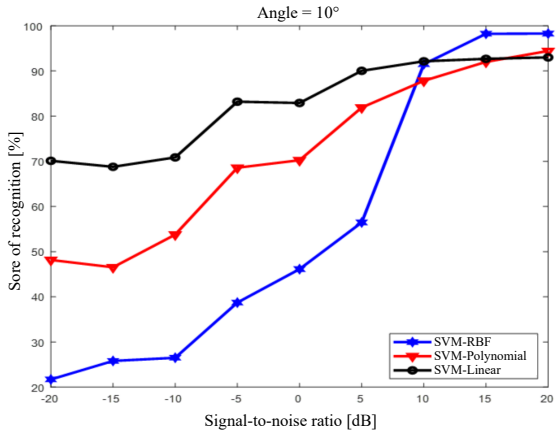

Fig. 9. Comparison of correct recognition rate for different SNR ratios at a 10° viewing angle for the three SVM classifier kernels.

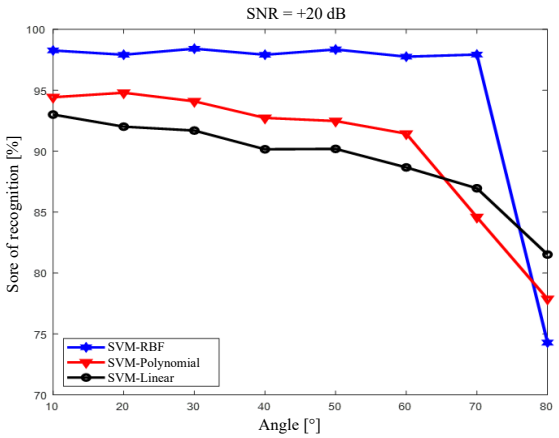

Fig. 10. Comparison of correct recognition rate for different viewing angles at SNR = 20 dB for the three SVM classifier kernels.

For a more comprehensive comparison, Table 4 presents the target recognition results using MLP-BP and MLP-GWO.

Table 4. The results of the classification with the classifiers MLP-BP and MLP-GWO.

SNR [dB]	Classifier	Angle 10°	Angle 20°	Angle 30°	Angle 40°	Angle 50°	Angle 60°	Angle 70°	Angle 80°
20	MLP-BP	13.60	19.60	20.00	15.10	16.80	18.39	14.43	11.22
	MLP-GWO	17.13	17.00	16.26	17.00	17.00	17.00	13.03	13.01
15	MLP-BP	14.39	11.66	13.60	8.79	11.61	12.40	7.19	5.6
	MLP-GWO	17.18	17.16	17.00	17.00	17.14	17.01	13.57	13.02
10	MLP-BP	11.51	11.62	10.41	9.94	8.42	7.12	8.82	7.83
	MLP-GWO	17.17	17.05	17.01	17.04	17.02	17.01	13.00	13.00
5	MLP-BP	8.41	9.34	4.00	8.46	10.81	9.63	6.47	7.19
	MLP-GWO	17.16	17.55	17.01	17.27	17.02	17.00	13.03	12.87
0	MLP-BP	7.19	7.87	5.20	7.19	6.80	4.39	4.39	4.80
	MLP-GWO	17.16	17.01	17.27	17.26	17.01	17.00	13.00	12.34
−5	MLP-BP	3.21	4.00	5.62	6.40	6.00	4.00	5.20	5.20
	MLP-GWO	17.14	17.40	17.40	17.01	17.40	17.02	13.01	13.00
−10	MLP-BP	3.60	2.80	4.00	7.60	6.00	4.00	2.41	4.82
	MLP-GWO	17.13	17.14	17.20	17.01	17.06	17.03	16.35	16.07
−15	MLP-BP	3.15	4.39	2.82	4.00	3.20	4.00	6.89	3.20
	MLP-GWO	16.07	16.80	15.62	16.71	14.80	14.75	14.68	13.80
−20	MLP-BP	3.20	4.12	5.69	3.20	5.61	5.54	3.11	3.59
	MLP-GWO	15.00	15.87	15.28	13.94	13.96	13.67	13.69	12.94

As shown in Table 4, MLP-BP has shown poor performance. The results for MLP-GWO are better than MLP-BP. However, in both classifiers, the results are not satisfactory. One of the reasons for the poor performance of neural networks is the number of classes. Obviously, increasing the number of classes causes an increase in the probability of errors and, as a result, a decrease in performance.

6. Conclusion

This paper uses a new method of using sonar micro-Doppler to automatically detect moving sonar targets. In other words, when the signal hits the propeller, each propeller has a unique effect on the signal according to its own metrics. Then, by transferring the signal to the frequency domain, its useful properties were extracted. Movable sonar targets were classified using linear kernels, RBF and polynomial SVM classifiers. The simulation results showed that the RBF kernel is significantly suitable for positive signal-to-noise ratios. For values with more noise, the linear kernel has different and significant performance compared to the other two kernels. Using GWO algorithm for neural network training improved the performance of the classifier compared to using BP for training, but overall, the result of using neural networks was not satisfactory. Therefore, the approach of using neural network is not suitable for this problem. However, due to the new idea of using sonar micro-Doppler to classify moving targets, the need to consider other machine learning methods and artificial intelligence techniques to improve the classifier performance in all SNRs and viewing angles is strongly noticeable.

Some of the topics that will be explored for future research are as follows:

- improving the performance of SVM classifiers using metaheuristic algorithms;
- use other machine learning algorithms to improve accuracy;
- use of hybrid classifiers to achieve more accurate accuracy for sensitive applications;
- use deep learning to improve classifier performance.

References

1. Anderson S.J. (2004), Target classification, recognition and identification with HF radar, [in:] *RTO SET Symposium on Target Identification and Recognition Using RF Systems*, pp. 1–20.
2. Berthold T., Leichter A., Rosenhahn B., Berkhahn V., Valerius J. (2018), Seabed sediment classification of side-scan sonar data using convolutional neural networks, [in:] *2017 IEEE Symposium Series on Computational Intelligence (SSCI)*, pp. 1–8, doi: 10.1109/SSCI.2017.8285220.
3. Bhanu B. (1986), Automatic target recognition: State of the art survey, *IEEE Transactions on Aerospace and Electronic Systems*, **22**(4): 364–379, doi: 10.1109/TAES.1986.310772.
4. Cai X. *et al.* (2021), Dynamically controlling terahertz wavefronts with cascaded metasurfaces, *Advanced Photonics*, **3**(3): 036003, doi: 10.1117/1.AP.3.3.036003.

5. Chen B. *et al.* (2022), DPM-LES investigation on flow field dynamic and acoustic characteristics of a twin-fluid nozzle by multi-field coupling method, *International Journal of Heat and Mass Transfer*, **192**: 122927, doi: 10.1016/j.ijheatmasstransfer.2022.122927.

6. Chen H., Li S. (2022), Collinear nonlinear mixed-frequency ultrasound with FEM and experimental method for structural health prognosis, *Processes*, **10**(4): 656, doi: 10.3390/pr10040656.

7. Chen V.C., Tahmoush D., Miceli W.J. (2014), *Radar Micro-Doppler Signature: Processing and Applications*, Institution of Engineering and Technology.

8. Clemente C., Balleri A., Woodbridge K., Soraghan J.J. (2013), Developments in target micro-Doppler signatures analysis: Radar imaging, ultrasound and through-the-wall radar, *EURASIP Journal on Advances in Signal Processing*, **2013**: 47, doi: 10.1186/1687-6180-2013-47.

9. Dong J., Deng R., Quanying Z., Cai J., Ding Y., Li M. (2021), Research on recognition of gas saturation in sandstone reservoir based on capture mode, *Applied Radiation and Isotopes*, **178**: 109939, doi: 10.1016/j.apradiso.2021.109939.

10. Ehrman L.M., Lanterman A.D. (2020), Incorporation of aircraft orientation into automatic target recognition using passive radar, *IET Radar, Sonar & Navigation*, **14**(7): 1079–1087, doi: 10.1049/iet-rsn.2020.0010.

11. Foued C., Ammar M., Arezki Y. (2017), Detection and classification of ground targets using a Doppler RADAR, [in:] *2017 Seminar on Detection Systems Architectures and Technologies (DAT)*, pp. 1–8, doi: 10.1109/DAT.2017.7889168.

12. Gaye B., Zhang D., Wulamu A. (2021), Improvement of support vector machine algorithm in big data background, *Mathematical Problems in Engineering*, **2021**: 5594899, doi: 10.1155/2021/5594899.

13. Glover F., Laguna M. (2008), *Principles of Tabu Search*, Springer Science.

14. Jin C. *et al.* (2020), Development and evaluation of an artificial intelligence system for COVID-19 diagnosis, *Nature Communications*, **11**: 5088, doi: 10.1038/s41467-020-18685-1.

15. Kaveh M., Khishe M., Mosavi M.R. (2019), Design and implementation of a neighborhood search biogeography-based optimization trainer for classifying sonar dataset using multi-layer perceptron neural network, *Analog Integrated Circuits and Signal Processing*, **100**(2): 405–428, doi: 10.1007/s10470-018-1366-3.

16. Kavzoglu T., Colkesen I. (2009), A kernel functions analysis for support vector machines for land cover classification, *International Journal of Applied Earth Observation and Geoinformation*, **11**(5): 352–359, doi: 10.1016/j.jag.2009.06.002.

17. Kazimierski W., Zaniewicz G. (2021), Determination of process noise for underwater target tracking with forward looking sonar, *Remote Sensing*, **13**(5): 1014, doi: 10.3390/rs13051014.

18. Khishe M., Mohammadi H. (2019), Passive sonar target classification using multi-layer perceptron trained by salp swarm algorithm, *Ocean Engineering*, **181**: 98–108, doi: 10.1016/j.oceaneng.2019.04.013.

19. Khishe M., Mosavi M.R. (2019), Improved whale trainer for sonar datasets classification using neural network, *Applied Acoustics*, **154**: 176–192, doi: 10.1016/j.apacoust.2019.05.006.

20. Khishe M., Safari A. (2019), Classification of sonar targets using an MLP Neural Network trained by Dragonfly Algorithm, *Wireless Personal Communications*, **108**: 2241–2260, doi: 10.1007/s11277-019-06520-w.

21. Koturwar P., Girase S., Mukhopadhyay D. (2015), A survey of classification techniques in the area of big data, *Computer Science*, pp. 1–7.

22. Lakhwani K. (2020), Big data classification techniques: A systematic literature, *Journal of Natural Remedies*, **21**(2).

23. Liu J., Zhou Z., Zeng X. (2019), Multi-static active sonar target recognition method based on bionic signal, [in:] *2019 IEEE 2nd International Conference on Information Communication and Signal Processing (ICICSP)*, pp. 285–289, doi: 10.1109/ICICSP48821.2019.8958532.

24. Mamgain R., Jain R., Deb D. (2018), Study and Simulation of Radar Targets' Micro-Doppler Signature, [in:] *2018 International Conference on Radar (RADAR)*, pp. 1–5, doi: 10.1109/RADAR.2018.8557264.

25. Molchanov P.O., Astola J.T., Egiazarian K.O., Totsky A.V. (2013), Classification of ground moving targets using bicepstrum-based features extracted from Micro-Doppler radar signatures, *EURASIP Journal on Advances in Signal Processing*, **2013**(1): 1–13, doi: 10.1186/1687-6180-2013-61.

26. Qiao W., Khishe M., Ravakhah S. (2021), Underwater targets classification using local wavelet acoustic pattern and Multi-Layer Perceptron neural network optimized by modified Whale Optimization Algorithm, *Ocean Engineering*, **219**: 108415, doi: 10.1016/j.oceaneng.2020.108415.

27. Saffari A., Khishe M., Zahiri S. (2022a), Fuzzy-ChOA: An improved chimp optimization algorithm for marine mammal classification using artificial neural network, *Analog Integrated Circuits and Signal Processing*, **111**: 403–417, doi: 10.1007/s10470-022-02014-1.

28. Saffari A., Zahiri S., Khishe M. (2022b), Automatic recognition of sonar targets using feature selection in micro-Doppler signature, *Defence Technology*, doi: 10.1016/j.dt.2022.05.007.

29. Saffari A., Zahiri S.H., Khishe M. (2022c), Fuzzy grasshopper optimization algorithm: A hybrid technique for tuning the control parameters of GOA using Fuzzy System for big data sonar classification, *Iranian Journal of Electrical and Electronic Engineering*, **18**(1): 1–13, doi: 10.22068/IJEEE.18.1.2131.

30. Saffari A., Zahiri S.H., Khishe M. (2022d), Fuzzy whale optimisation algorithm: A new hybrid approach for automatic sonar target recognition, *Journal of Experimental & Theoretical Artificial Intelligence*, doi: 10.1080/0952813X.2021.1960639.
31. Sclavounos P.D., Ma Y. (2018), Artificial intelligence machine learning in marine hydrodynamics, [in:] *Proceedings of the ASME 2018 37th International Conference on Ocean, Offshore and Arctic Engineering. Volume 9: Offshore Geotechnics; Honoring Symposium for Professor Bernard Molin on Marine and Offshore Hydrodynamics*, doi: 10.1115/OMAE2018-77599.
32. Smith G.E., Woodbridge K., Baker C.J. (2007), Multiperspective micro-Doppler signature classification, [in:] *IET International Conference on Radar Systems 2007*, doi: 10.1049/cp:20070522.
33. Tahmoush D. (2015), Review of micro-Doppler signatures, *IET Radar, Sonar & Navigation*, **9**(9): 1140–1146, doi: 10.1049/iet-rsn.2015.0118.
34. Uddin S., Khan A., Hossain M.E., Moni M.A. (2019), Comparing different supervised machine learning algorithms for disease prediction, *BMC Medical Informatics and Decision Making*, **19**: 281, doi: 10.1186/s12911-019-1004-8.
35. Waite A.D. (2002), *Sonar for Practising Engineers*, Wiley.
36. Wawrzyniak N., Stateczny A. (2017), MSIS image postioning in port areas with the aid of comparative navigation methods, *Polish Maritime Research*, **24**(1): 32–41, doi: 10.1515/pomr-2017-0004.
37. Wu C., Khishe M., Mohammadi M., Taher Karim S.H., Rashid T.A. (2021), Evolving deep convolutional neutral network by hybrid sine–cosine and extreme learning machine for real-time COVID19 diagnosis from X-ray images, *Soft Computing*, doi: 10.1007/s00500-021-05839-6.
38. Xu H., Zhou J., Asteris P.G., Armaghani D.J., Tahir M.M. (2019), Supervised machine learning techniques to the prediction of tunnel boring machine penetration rate, *Applied Sciences*, **9**(18): 3715, doi: 10.3390/app9183715.
39. Yang Y., Lei J., Zhang W., Lu C. (2006), Target classification and pattern recognition using micro-Doppler radar signatures, [in:] *Seventh ACIS International Conference on Software Engineering, Artificial Intelligence, Networking, and Parallel/Distributed Computing (SNPD'06)*, pp. 213–217, doi: 10.1109/SNPD-SAWN.2006.68.
40. Zhang T., Liu S., He X., Huang H., Hao K. (2020), Underwater target tracking using forward-looking sonar for autonomous underwater vehicles, *Sensors*, **20**(1): 102, doi: 10.3390/s20010102.
41. Zhong T., Cheng M., Lu S., Dong X., Li Y. (2022), RCEN: A deep-learning-based background noise suppression method for DAS-VSP records, [in:] *IEEE Geoscience and Remote Sensing Letters,* **19**: 3004905, doi: 10.1109/LGRS.2021.3127637.
42. Zhou J., Bai J., Liu Y. (2022), Fabrication and modeling of matching system for air-coupled transducer, *Micromachines*, **13**(5): 781, doi: 10.3390/mi13050781.